Nanoscale

Cite this: *Nanoscale*, 2012, **4**, 7362

www.rsc.org/nanoscale

COMMUNICATION

Fabrication of cone-shaped CNF/SiC-coated Si-nanocone composite structures and their excellent field emission performance

I-Ju Teng,*[ad] Hui-Lin Hsu,[b] Sheng-Rui Jian,*[c] Cheng-Tzu Kuo[a] and Jenh-Yih Juang*[d]

Received 16th June 2012, Accepted 8th October 2012
DOI: 10.1039/c2nr31511d

Novel cone-shaped carbon nanofiber (CNF)/silicon carbide (SiC)-coated Si-nanocone (Si-NC) composite structures with excellent field emission (FE) performance have been fabricated by a simple microwave plasma chemical vapour deposition process. Transmission electron microscopy analyses reveal that the newly developed cone-shaped composite structures are composed of bamboo-like herringbone CNFs grown vertically on the tips of conical SiC layers with a flat-top Si cone embedded underneath. For this CNF/SiC-coated Si-NC composite array, a ultra-low threshold field of 0.32 V μm^{-1} (at 10 mA cm^{-2}), a large emission current density of 668 mA cm^{-2} at 1.05 V μm^{-1}, and a field enhancement factor as high as ~48 349 are obtained. In addition, the FE lifetime test performed at a large emission current density of 200 mA cm^{-2} under an applied field of 1 V μm^{-1} shows no discernible decay during a period of over 260 minutes. We deduce that this superior FE performance can be attributed to the specific bamboo-like herringbone CNFs with numerous open graphitic edges and a faceted top end, and the conical base SiC/Si structures with sufficient adhesion to the substrate surface. Such a novel structure with promising emission characteristics makes it a potential material for electron field emitters.

Introduction

The unique properties exhibited by carbon nanofibers (CNFs) and carbon nanotubes (CNTs), such as the large aspect ratio, small tip radius of curvature, high emission current density, superior electrical/thermal conductivity, robust mechanical strength, and good chemical stability, have made these nanomaterials the choice of electron field emitters such as field emission displays, lighting lamps, X-ray sources, *etc.*[1] However, owing to the adherence, shielding and shape issues frequently encountered by the CNTs and CNFs directly grown on various substrates with or without catalysts, the lifetime and reproducibility of the emitters made of CNTs and CNFs still remain two of the major challenges. To overcome these obstacles and/or further enhance nanostructure field emission (FE) properties, new forms of CNTs or CNFs[2–7] as well as composite structures with CNTs/CNFs or carbon nanosheets attached/grown on the tips or surfaces of conical bases have been proposed.[8–17] So far, the reported synthesis methods about the new type of carbon-based composites suitable for FE applications typically require multiple-step processes, time-consuming sample preparation, and/or lithographical patterning.[8–17] It is thus of interest to develop a simple and efficient method for directly fabricating a new carbon-nanomaterial/nanocone composite structure with excellent FE performances.

In this paper, we report on the FE properties of a novel cone-shaped CNF/silicon carbide (SiC)-coated Si-nanocone (Si-NC) composite structure *in situ* fabricated by a single step microwave plasma chemical vapour deposition (MPCVD) method without the use of any complicated lithography/etching techniques and pre-patterned templates. Furthermore, the detailed morphological and structural features of the newly developed cone-shaped composite structures are analyzed and discussed with respect to their excellent FE performance in terms of low threshold field, large field enhancement factor (β), and high emission current density. The promising FE performances suggest a great potential of the proposed CNF/SiC-coated Si-NC composite structure as a competitive candidate for future field emitters.

Experimental

A 10 nm thick Fe film was deposited onto Si wafers as a catalyst layer by sputtering. Prior to deposition processes, the as-deposited Fe-coated Si substrates were pretreated with hydrogen plasma for 10 minutes in the MPCVD chamber operated at 100 sccm H_2 while keeping the chamber pressure at 9 Torr, and the plasma power at 400 W. The CH_4–H_2 (1–100 sccm–sccm) gas was subsequently introduced into the chamber to ignite the CH_4–H_2 mixed plasma at 750 W. Nanostructures were grown on the Fe/Si substrates biased at −320 V and the deposition time was varied from 1 to 40 min. The substrates were not heated intentionally and the growth temperature during MPCVD processes was monitored closely to be around 345 °C at the first minute and then gradually increased to 630 °C after 10 minutes.

The surface morphology and microstructure of the as-grown samples were characterized by using field-emission scanning electron microscopy (FESEM, JEOL-6500) and high-resolution transmission

[a]*Department of Materials Science and Engineering, National Chiao Tung University, Hsinchu 30010, Taiwan. E-mail: ijteng@nctu.edu.tw*
[b]*Department of Electrical and Computer Engineering, University of Toronto, Toronto M5S 3G4, Canada. E-mail: huilin.hsu@mail.utoronto.ca*
[c]*Department of Materials Science and Engineering, I-Shou University, Kaohsiung 84041, Taiwan. E-mail: srjian@gmail.com*
[d]*Department of Electrophysics, National Chiao Tung University, Hsinchu 30010, Taiwan. E-mail: jyjuang@cc.nctu.edu.tw*

electron microscopy (HRTEM, JEM-2100F). A micro-Raman spectroscope (Jobin Yvon LabRam HR) with 514.5 nm (2.41 eV) and 632.8 nm (1.96 eV) laser line excitation sources was employed to identify the characteristics of as-grown nanostructures. The FE properties of as-grown samples were determined in a vacuum chamber at a pressure of less than 10^{-6} Torr using a simple diode configuration. The distance between the anode and the emitting surface is about 100 μm, which is controlled by a precision screw meter, and the emission measurement area is estimated to be about 3.2 mm^2. A high voltage source-measure unit (Keithley 237) was used to provide variable dc voltages and collect electric current across tested samples.

Results and discussion

Synthesis and characterization

Fig. 1(a)–(f) are the SEM images showing the morphological evolution of the nanostructures formed at various deposition stages corresponding to different deposition durations. As shown in Fig. 1(a), within the first minute of deposition, only nano-sized islands, resulting from the fragmentation of the Fe catalyst layer, with irregular shapes and different sizes are formed, while no apparent cone-shaped structures are observed at this stage. As the deposition time is prolonged to 3 min (Fig. 1(b)), densely packed nanocones of ~97 nm in length, ~49 nm in base-diameter, ~10 nm in tip radius and ~2.0 in aspect ratio (defined as a ratio of the as-produced nanostructure's total length to its base-diameter) are formed with catalytic Fe-based nanoparticles sitting on their tips. It is noted that at these stages the Raman spectra (not shown here) display only a broad plateau covering the range between 1200 and 1700 cm^{-1}, indicating

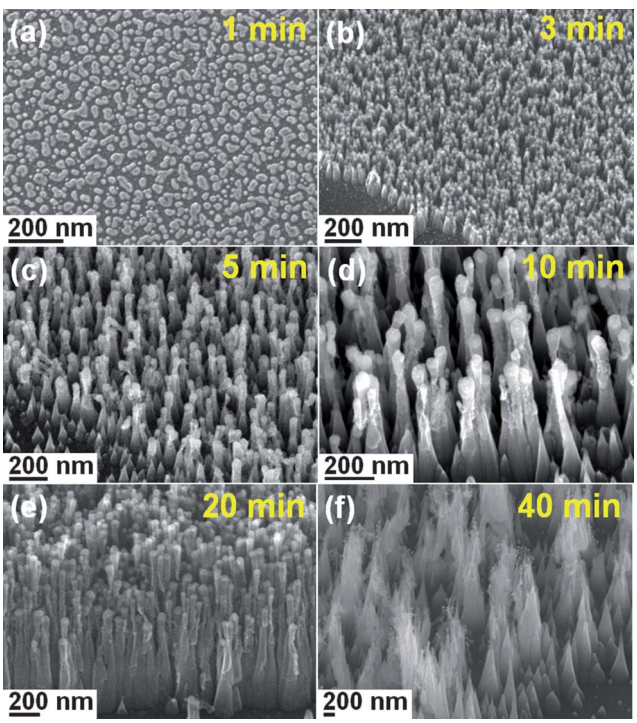

Fig. 1 SEM images of the nanostructures synthesized on Fe/Si substrates at the deposition times of (a) 1 min, (b) 3 min, (c) 5 min, (d) 10 min, (e) 20 min, and (f) 40 min, respectively.

that the nanocones would be mainly Si-containing structures masked by Fe-based nanoparticles and no discernible CNFs or CNTs are formed. This is quite different from those reported previously[9,10] wherein the nanocones were suggested to result from the coalescence of CNF bundles originally formed on Co/Al/Si substrates pretreated with hydrogen plasma. On the other hand, as pointed out by Chen *et al.*[11] that, at a bias voltage of above 550 V during a dc plasma enhanced CVD process, nanocones were formed due to sputtering-induced continuous reduction in the size of Ni catalyst particles, which eventually limited the vertical growth while lateral coarsening occurred continuously at the expense of neighboring nanocones. Nonetheless, the energy dispersive X-ray spectroscopy analysis revealed that such nanocones did contain some Si,[11] indicating that the early stage growth mechanism of the nanocones in the proposed structures may be more complex than previously conceived.[9,10]

A further increase of the deposition time, however, results in apparent morphology evolutions in as-produced nanostructures. As displayed in Fig. 1(c)–(e), the average length of the underneath nanocones increases from 139 nm to 344 nm with increasing deposition time from 5 min to 20 min; meanwhile their base size is found to increase from 76 nm (5 min) to 130 nm (20 min). Moreover, it is noted that filament-like structures of ~36 nm in diameter commence to grow vertically upward from the tips of the nanocones to develop a "filament-on-nanocone" configuration after 5 min deposition time (Fig. 1(c)). The filaments continue to evolve with increasing deposition time, becoming longer and denser, and furthermore they start to assemble into straight bundles, as shown in Fig. 1(d). As the deposition time is increased to 20 min (Fig. 1(e)), these bundles grow longer to reach ~350 nm with the number density being increased to ~3×10^{10} cm^{-2} and only minor variation in the diameter compared to their length. Additionally, for the nanostructures deposited at 5 minutes up to 20 minutes an improved filament aspect ratio from ~2.7 to ~10.9 and a "filament-on-nanocone" aspect ratio from ~3.1 to ~5.4 are obtained, which is expected to further improve the FE characteristics of the newly developed cone-shaped composite structures. However, by prolonging the deposition time to 40 min, most of the filaments and underneath nanocones appear to be subjected to significant plasma etching, giving rise to a structural morphology consisting of sharpened nanocones and residual filaments sparsely existing on the tips of some severely damaged nanocones, as exhibited in Fig. 1(f). The morphological features of the representative nanostructures are given in Table 1. The above results suggest that appropriate manipulation of the deposition time could lead to "filament-on-nanocone" composite structures with different combinations of dimensions and densities, which is desirable for various electronic device applications.

In order to elucidate the detailed structural features of the filaments grown on the tips of the nanocone arrays, TEM analyses are performed on the 20 min sample (Fig. 1(e)). Although the samples obtained with specifically selected synthesis parameters practiced in our MPCVD system are chosen for this purpose, the features revealed should be representative in general. It can be seen from Fig. 2(a) that filament bundles are formed on the top of nanocones, as schematically indicated by the orange circle (*vide infra*). The nanocones, on the other hand, appear to consist of two parts, namely a flat-top cone embedded in a more sharpened cone, as schematically depicted by the blue lines and red lines in Fig. 2(a), respectively. The selected area electron diffraction (SAED) pattern and the HRTEM image taken from the underneath flat-top cone indicate that it is essentially single crystal Si with a clear Si (111) lattice spacing

Table 1 The geometrical characteristics and the field emission properties of the samples under investigation

	Carbon nanofiber (CNF) average properties			Nanocone (NC) average properties			Field emission properties			
Sample ID[a]	Length (l, nm)/ diameter ($2r$, nm)	Aspect ratio	Density ($\times 10^9$ cm^{-2})	Length (L, nm)	Base-diameter (D, nm)	CNF-on-NC aspect ratio[b]	E_{th}[c] (V μm^{-1})	J[d] (mA cm^{-2})	β[e]	β_{FN}[f]
1 min	n/a/n/a	n/a	n/a	n/a	n/a	n/a	n/a	n/a	n/a	n/a
3 min	n/a/n/a	n/a	n/a	97	49	~2.0	n/a	4×10^{-7}	~10	~1622
5 min	97/36	2.7	7.4	139	76	~3.1	0.61	185	~13	~25 277
10 min	163/33	5.0	15.6	285	105	~4.3	0.35	273	~27	~33 197
20 min	349/32	10.9	28.8	344	130	~5.4	0.32	>668	~43	~48 349
40 min	n/a/n/a	n/a	n/a	1439	405	~3.5	10	4×10^{-5}	~86	~1231

[a] Nanostructure deposition time. [b] The ratio of the as-produced nanostructure's total length to its base-diameter, $(l + L)/D$. [c] Threshold electric field for an emission current density of 10 mA cm^{-2}. [d] Emission current density at an electric field of 1.05 V μm^{-1}. [e] Field enhancement factor calculated using $\beta \approx$ nanostructure's total length/tip radius. [f] Field enhancement factor derived from F–N plots.

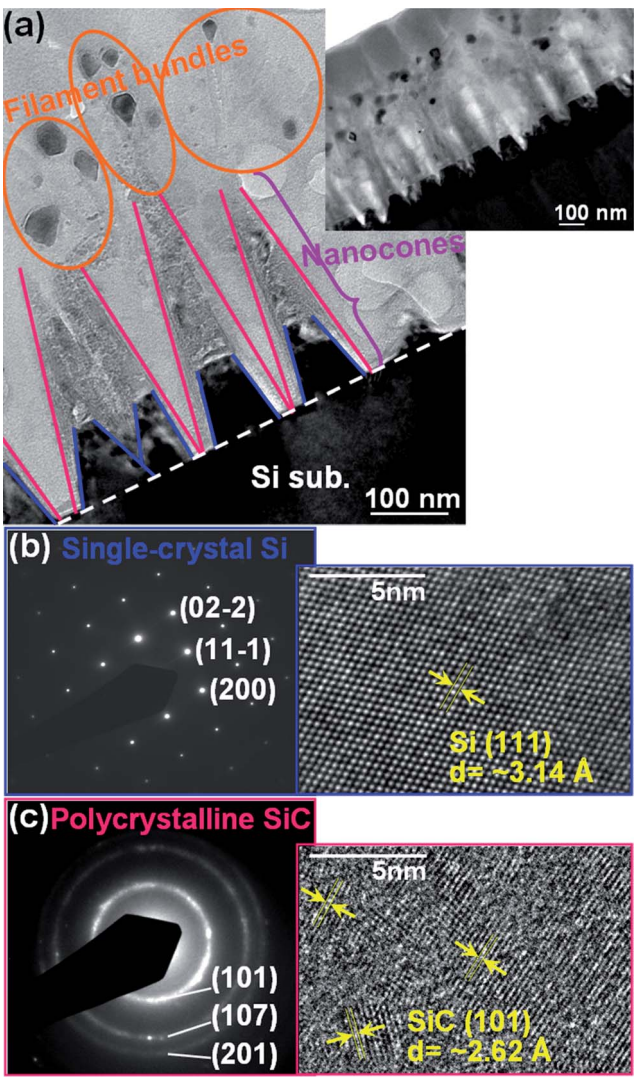

Fig. 2 (a) Cross-sectional TEM image for the CNF/SiC-coated Si-NC composite structures obtained with our MPCVD system. SAED patterns and lattice images taken from the (b) lower base part and (c) upper part of the nanocones displayed in (a).

of ~3.14 Å, as displayed in Fig. 2(b). Nevertheless, the SAED pattern taken from the outer part of the nanocones exhibits the typical ring pattern of polycrystalline structures (Fig. 2(c)). The three diffraction rings shown in Fig. 2(c) can be indexed to the reflections of (101), (107) and (201) planes of 6H-SiC according to the Joint Committee on Powder Diffraction Standards (JCPDS) data (Card Files, no.72-0018). Furthermore, their HRTEM image shows a lattice spacing of ~2.62 Å which is very close to the spacing of the (101) plane for the hexagonal lattice of 6H-SiC structures. However, the phases and compositions of the obtained SiC nanocones need further detailed investigations.

In addition, as shown in Fig. 3(a)–(c), the HRTEM images taken from a single filament on nanocone tips reveal that the plane of graphite sheets is at an angle with respect to the filament axis comprising of bamboo-like compartments, and a faceted catalyst particle with sharp corners is encapsulated inside the filament's top end. The average lattice spacing of the filament walls is about 3.35 Å which is close to that of the single crystal graphite. This type of filaments is generally referred to as bamboo-like fishbone or herringbone CNFs grown by the catalysis-driven tip-growth mechanism.[18] Furthermore, it should be noted that there are many open ends of graphite sheets existing on the surface of the CNF as indicated by black arrows in Fig. 3(b) and (c). This open-end graphite surface structure is expected to play a significant role in determining the unusual electrical properties of these nanofibers. The above TEM analyses thus indicate that the entire cone-shaped composite structures obtained by the present process are composed of vertically oriented CNF bundles and SiC/Si nanocones, as schematically depicted in Fig. 3(d). Although it has been proposed in the literature[6,19,20] that, during a plasma CVD process, the evolution of conical base structures is most likely caused by the competition between the growth rate (associated with carbon-containing species) and the sputter-etching effect (associated with ionic and neutral species bombardment) of growing nanostructures, our results seem to indicate otherwise. In our case, the particle size of the catalyst may be still too large at the early stages to initiate the CNF growth, and hence it may serve as the mask for plasma etching on the Si substrate, which may be also accompanied by SiC formation and give rise to SiC/Si-nanocone structures. As the size of catalyst particles reaches some critical size after prolonged plasma bombardment, CNFs can thus commence to grow on the tips of the SiC/Si nanocones *via* the tip-growth mechanism with the assistance of the Fe-based nanoparticles

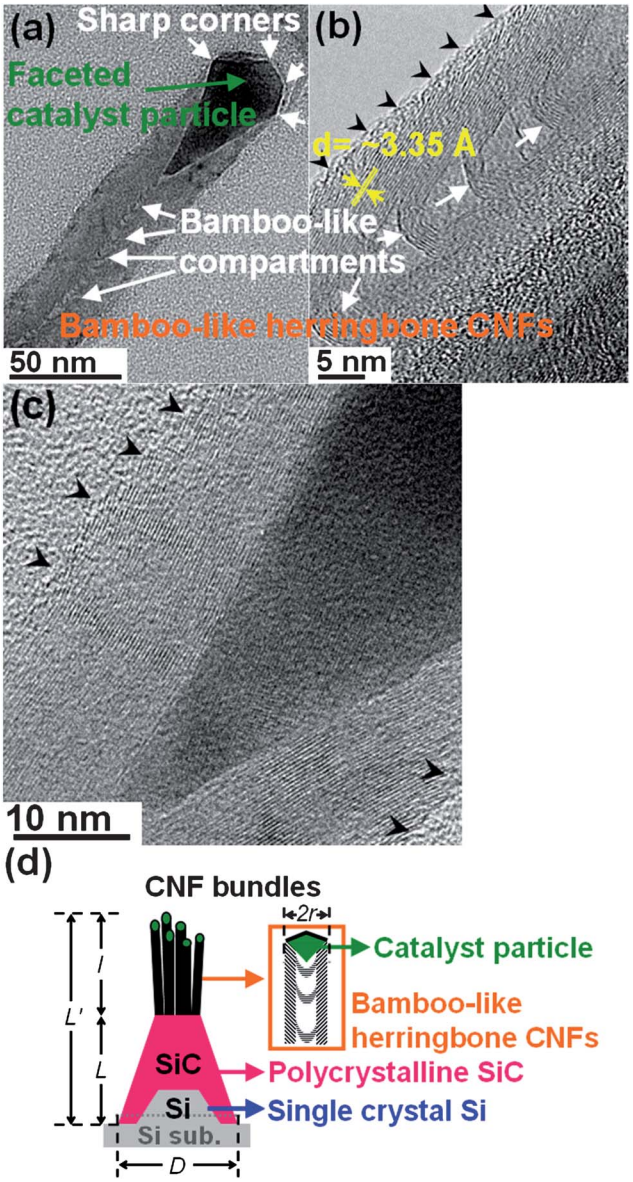

Fig. 3 (a–c) HRTEM images of a single filament indicating a bamboo-like herringbone CNF with a faceted catalyst particle encapsulated inside its top end. Numerous open ends of graphite sheets existing on the CNF surface (indicated by black arrows). (d) Schematic diagram for the cone-shaped composite structure of vertically oriented CNF bundles grown on SiC/Si-nanocones in our experiment.

remaining on the tips. The details of the mechanism behind the formation of the unique CNF/nanocone combined structures though may still need further experiments to verify, such as varying the initial size of the catalyst particles, the CNF/SiC-coated Si-NC composite structures, nevertheless, represent a structure which has never been reported before. Thus, it should be interesting to further investigate the FE properties exhibited by these newly developed cone-shaped composite structures.

Field electron emission *J–E* characteristics

Fig. 4 displays the typical current density *versus* electric field (*J–E*) curves of the samples prepared at different deposition times. The

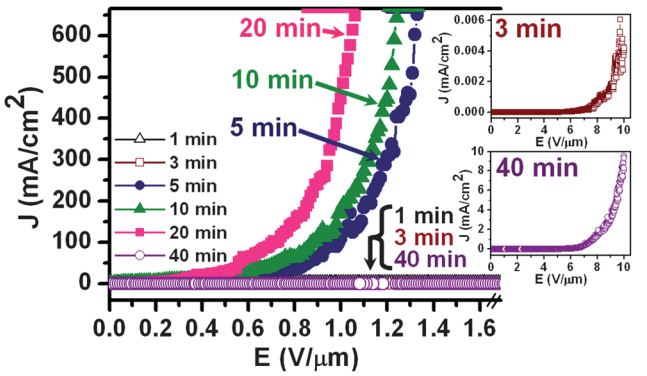

Fig. 4 Field emission *J–E* curves of the samples prepared at different deposition times.

threshold field (E_{th}), defined as the applied field required for obtaining an emission current density of 10 mA cm^{-2}, of the nanostructures grown for 5, 10 and 20 min is 0.61, 0.35 and 0.32 V μm^{-1}, respectively, which is much lower than other carbon-related nanostructured emitters reported in the literature.[2–17] Moreover, for the sample with the best FE performance (20 min), a high emission current density of over 668 mA cm^{-2} is achieved at the applied field of merely 1.05 V μm^{-1}. On the other hand, the insets of Fig. 4 show the FE properties of the 3 min and 40 min samples with the applied electric field ranging from 0 to 10 V μm^{-1}, indicating that in these cases their E_{th} are substantially higher and J are much lower than those described above. Besides, for the 1 min sample (Fig. 1(a)), presumably due to the absence of desired geometry, there is no sign of emission within the maximum field range available to our facility. The comparison of the geometrical characteristics and the field emission properties of these samples are presented in Table 1.

From Table 1, it can be seen that the values of the E_{th} and J among these samples are closely related to the average length, aspect ratio and density of the vertically oriented CNFs residing on the tips of nanocones, but only weakly depend on the geometrical characteristics of the underneath nanocones. This statement is based on the observations that significant changes in the E_{th} and J are obtained as the nanostructure deposition time increases from 3 to 5 min and 20 to 40 min, respectively, and furthermore the 20 min sample shows much better FE performance in terms of lower E_{th} and higher J than 5 min and 10 min samples. In other words, the absence of the straight CNFs should be one predominant factor that results in the relatively poor emission characteristics with high E_{th} and low J values from the samples with only nanocone arrays (3 min and 40 min), even if the nanocones from the 40 min sample have a largest dimensional size and a comparable CNF-on-NC aspect ratio as indicated in Table 1. In the next section, we will discuss potential reasons behind the improvement of FE characteristics of the proposed CNF/SiC-coated Si-NC composite structures.

It has been shown recently that materials with elongated geometry,[21] increased emission sites,[22] sharp/protruded edges,[23] defective/disordered structures,[24] or lower local work function[25] can greatly enhance their FE properties. For our CNF/SiC-coated Si-NC composite structures prepared by 5–20 min, the samples contain bundles of CNFs on nanocone tips, where each nanofiber may be considered as an individual field emission site. Therefore, one of the reasons for the best emission characteristics obtained from the 20 min sample could be the optimized and/or maximized CNF aspect ratio

and the total number of emission sites on the sample surface primarily due to the increase in both length and density of the CNFs with the deposition time. Furthermore, it is worth noting that the present Fe-based catalyst particles encapsulated inside the top ends of the CNFs exhibit clearly defined facets with sharp edges, which also lead the cap of the CNFs to appear correlatively sharply faceted, as can be observed in Fig. 2(a) and 3(a). Earlier studies of diamond particles[26] and bamboo-like SiC nanowires[27] have demonstrated that nanostructures with fine facets may have ideally large curvatures and their sharp corners may serve as emitting centers as well. As a result, it is suggested that for our samples the existence of the faceted catalyst particles on the CNF top ends not only clearly indicates the tip growth mechanism for the CNFs, but also provides the sharp corners with extremely small radius of curvature, which may act as efficient electron emitting sites due to the strong local field enhancement at their surfaces, thereby greatly improving the FE efficiency. In order to have better agreement, FE measurement has also been carried out for the samples with the catalyst particle removed from the CNFs *via* plasma treatments and acid oxidation. However, discordant results are obtained from our preliminary tests among various morphologically and structurally reproducible samples as shown in Fig. 1(e). We attribute the instable and inconsistent FE performances to the difficulty in precise positioning treatment through these two processes, leading to the cone-shaped composite structures being damaged to some extent or broken/lost in some cases. In addition to these undesirable impact on the final cone-shaped structures, the serial treatment processes may cause the formation of chemical groups on the surface of the nanostructures and/or a drastic change in their electronic structure, which would significantly alter the work function of the samples and thus give rise to a large variation of the FE parameters between the samples tested.[28] Although there are still many challenges in the removal of the encapsulated catalyst particle from our CNFs, while still retaining the sample's general structural integrity, it is certainly necessary to clarify the correlation between the faceted catalyst particles and the performance improvement in our case. Continuing work on this topic and on fine-tuning the post-processing is underway in our group. Finally, as mentioned earlier, in this work the CNFs on nanocone tips are shaped into a herringbone structure, consisting of a number of bamboo-like compartments, which are believed to play a significant role in the improvement of FE properties.[29–37] This is because both herringbone-type and bamboo-type carbon fiber/tube structures contain many edge-plane-like defects/sites, where graphite sheets terminate on the outer walls of the fibers/tubes to form numerous open graphitic edges, and are therefore thought to contain more active sites at the surface, in addition to the area of the fiber/tube ends.[29–37] More precisely, since these open graphitic edges are very sharp and thin, they could generate strong local electric fields at their apexes, and would also account for substantial emission currents measured from nanostructures at relatively small local fields, thereby a superior FE performance could be expected.[29–37] Accordingly, we suggest that the open edge/defect emission mechanism is another dominant factor which results in the ultra-low threshold field and high emission current density obtained from our CNF/SiC-coated Si-NC composite structures. For this reason, it is also reasonable to expect that the 20 min sample with higher CNF density and larger fiber length on nanocone tips has more open graphitic edges and defects, and thus electron emission with a relatively low turn-on/threshold fields and a significantly improved emission current density can be achieved.

Estimation of field enhancement factor (β) values

In order to further delineate the emission mechanism prevailing in the CNF/SiC-coated Si-NC composite structures, the *J*–*E* curves are further analyzed on the basis of the classical Fowler–Nordheim (F–N) theory[38] with the following expression:

$$J = \left[\frac{(1.54 \times 10^{-6})\beta^2 E^2}{\varphi}\right] \exp\left[-\frac{(6.83 \times 10^{9})\varphi^{3/2}}{\beta E}\right] \quad (1)$$

where J, β, E, and φ are denoted as the emission current density, the geometric field enhancement factor of the emitter, the applied electric field, and the work function of the emitter, respectively. The F–N plots [$\ln(J/E^2)$ *versus* $1/E$] corresponding to the samples under investigation are depicted in Fig. 5(a). The linear relationship between $\ln(J/E^2)$ and $1/E$ in the low applied electric field region implies that the electron emission from these samples follows F–N behaviour. In addition, by considering a work function of CNFs of 5 eV,[12] the value of β_{FN}, estimated by fitting the linear part of their corresponding F–N plots, is found to be 1622, 25 277, 33 197, 48 349, and 1231 for 3, 5, 10, 20 and 40 min samples, respectively, as presented in Table 1. The obtained β_{FN} values for the 5, 10 and 20 min samples are substantially higher than most of the results obtained from various new forms of CNF/CNFs or carbon-based composites previously reported.[2–17] In an attempt to find possible explanations of such high β_{FN} values obtained here, a two-stage model is employed.[40–43] In a two-stage model the total field enhancement factor of emitters with the combination of two different sorts of nanostructures (one followed by another) is a product of the enhancement factors for individual stages.[40–43] Accordingly, β for our CNFs on the nanocone tip system can be presented as[40]

$$\beta_{tot} = \prod_{i=1}^{2} \beta_i = \beta_{CNF}\beta_{nanocone} = \frac{l}{(l+d)}\left(1+\frac{d}{r}\right)\frac{L'}{L'+d}\left(1+\frac{d}{R'}\right) \quad (2)$$

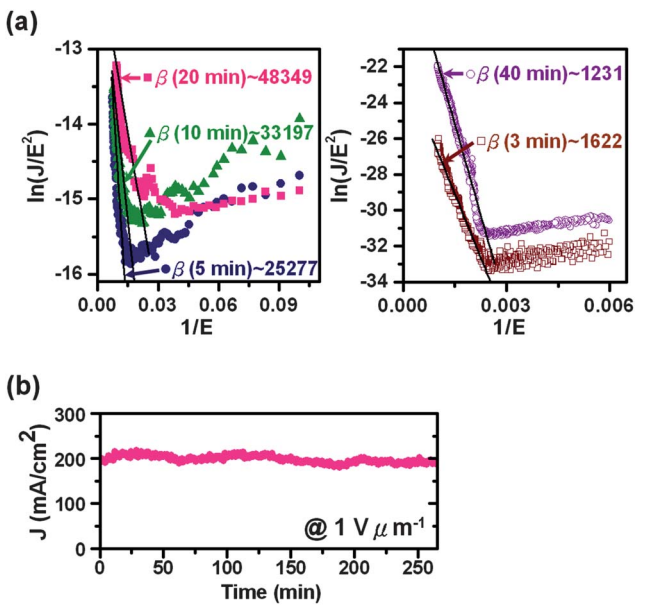

Fig. 5 (a) Corresponding F–N plots for the samples under investigation. (b) Emission current stability test performed on the 20 min sample at a constant applied electric field of 1 V μm^{-1}.

where l and r are the length and radius of the CNFs, while L and R are the length and radius of the underneath nanocones, and d is the inter-electrode spacing. $L' = L + l$ and $R' = R + l$ are the effective length and radius of the emitter, *i.e.* CNFs and nanocones in our case. Here, it is necessary to note that in this study the top CNF length is larger than the underneath nanocone radius (*i.e.* $l > R$). Therefore, based on the theoretical analysis of Huang *et al.*,[39] eqn (2) can now be simplified to

$$\beta_{\text{tot}} \approx L'/r \tag{3}$$

Consequently, the calculated β_{tot} value is ~13, ~27 and ~43 for the case of the 5, 10 and 20 min sample, respectively. Obviously, these values are much smaller than those derived from F–N plots. We consider that this significant discrepancy may be partly due to the existence of multi-stage units in our CNFs on the nanocone tip system rather than of only two-stage. That is, additional field enhancement may be generated by the very thin and sharp edges of the graphitic sheets terminating on the surface of the bamboo-like herringbone CNFs, as well as by the sharp corners at the top end of the faceted CNF/catalyst particles. As a result of the multi-stage field enhancement effect for the CNF/SiC-coated Si-NC composite structures with very fine, final stage edges, the total geometric enhancement factor becomes exceedingly high according to eqn (2). A high β value is favorable for electrons to overcome the surface potential barrier at relatively low applied electric fields, which in turn determines the total emission current. Hence, the highest field enhancement factor gives rise to the lowest threshold field and the largest emission current density of the 20 min sample, as can be observed in Fig. 4 and 5(a) and Table 1. A relatively larger β_{FN} is also observed even in the case of the 3 min and 40 min samples, suggesting the existence of smaller field enhancing sites on the structures. However, a relatively high threshold field and a low emission current density obtained indicate that the subsequent growth of CNF bundles on nanocone tips is surely advantageous to provide more atomically sharp emission sites for electron emission.

From the above results, we see that the β value for our CNF/SiC-coated Si-NC emitters is determined not only by the geometrical characteristics of the emitters, but also by the spatial density and the bamboo-like herringbone structure of the CNFs grown on the nanocone tips. Although it is difficult from our experiments to identify the exact distribution of individual emission centers, the β value provided by each multistage step, and the actual localized states of the emitting regions, the systematic and comparative analyses of the obtained experimental data have provided some qualitative information with respect to the remarkable improvement in FE characteristics, as evident from the ultra-low threshold field, enhanced emission current densities and high field enhancement factor, for the novel cone-shaped CNF/SiC-coated Si-NC composite structures. Further experiments are being performed to understand the cause of the high enhancement factor.

Emission current stability tests

The stability of the FE current over time is crucial for practical device applications, particularly for employing as cold cathode electron sources. Emission current for the best performing 20 min sample has been monitored over a long period of continuous operation at a fixed field of 1 V μm^{-1}, as shown in Fig. 5(b). It is clear that the emission current density reaches 200 mA cm^{-2} and is stable for over 260 minutes without discernible degradation. This good emission stability has also demonstrated that a strong adhesion of the CNF/SiC-coated Si-NC composite structures to the bottom Si substrate is achieved as a result of the conical base SiC/Si structures, which is a prerequisite for an excellent field emitter. The slight fluctuation of emission current density observed may be due to the absorption and desorption of molecules to nanostructure tips in a vacuum chamber during electron emission.[44] The high emission current density obtained at relatively lower applied fields as well as the good long term stability achieved make the proposed cone-shaped CNF/SiC-coated Si-NC composite structures a promising candidate material for high performance field emitting devices.

Conclusions

In summary, we have demonstrated a novel cone-shaped composite structure consisting of bamboo-like herringbone CNFs grown vertically on the tips of SiC-coated Si nanocones, and investigated their FE properties. The unique CNF/nanocone combined structure is directly fabricated onto Si substrates by a simple MPCVD process without the use of any complicated lithography/etching techniques and pre-patterned templates. Their FE measurement results reveal that the as-produced CNF/SiC-coated Si-NC composite structures possess remarkable FE characteristics with a ultra-low threshold field of ~0.32 V μm^{-1}, a large emission current density (over 668 mA cm^{-2} at an applied field of 1.05 V μm^{-1}), and a high field enhancement factor (over 48 349). Moreover, the FE stability of the best behaved sample is tested at a constant electric field of 1 V μm^{-1}, and no obvious degradation of an emission current density of 200 mA cm^{-2} is observed over 260 minutes. The specific bamboo-like herringbone CNFs with numerous open graphitic edges and a faceted top end, as well as the conical base SiC/Si structures with sufficient adhesion to the substrate surface, are considered to account for the excellent FE characteristics of the CNF/SiC-coated Si-NC composite arrays. Our results indicate that considerable improvement in the performance of electron field emitters could be achieved by incorporating the newly developed cone-shaped composite structures into devices.

Acknowledgements

This work was supported by Taiwan National Science Council under project number NSC100-2221-E-214-024 and by MOE ATU program at NCTU. The authors acknowledge the facility support provided by MSE department, CNST, and NFC at NCTU.

Notes and references

1 A. V. Eletskii, *Phys.-Usp.*, 2010, **53**, 863.
2 X. Calderón-Colón, H. Geng, B. Gao, L. An, G. Cao and O. Zhou, *Nanotechnology*, 2009, **20**, 325707.
3 S. H. Lim, H. S. Kim, C. H. Lee, S. M. Pietruszko and J. Jang, *J. Non-Cryst. Solids*, 2002, **299**, 864.
4 I. Sameera, R. Bhatia, V. Prasad and R. Menon, *J. Appl. Phys.*, 2012, **111**, 044307.
5 K. S. Hazra, P. Rai, D. R. Mohapatra, N. Kulshrestha, R. Bajpai, S. Roy and D. S. Misra, *ACS Nano*, 2009, **3**, 2617.
6 J. J. Li, Q. Wang and C. Z. Gu, *Ultramicroscopy*, 2007, **107**, 861.
7 C. H. Weng, K. C. Leou, H. W. Wei, Z. Y. Juang, M. T. Wei, C. H. Tung and C. H. Tsai, *Appl. Phys. Lett.*, 2004, **85**, 4732.
8 W. F. Jiang, H. S. Hao, Y. S. Wang, L. Xu and T. J. Zhang, *Appl. Surf. Sci.*, 2011, **257**, 633.

9 C. M. Yeh, M. Y. Chen, J. Hwang, J. Y. Gan and C. S. Kou, *Nanotechnology*, 2006, **17**, 5930.
10 C. J. Huang, C. M. Yeh, M. Y. Chen, J. Hwang and C. S. Kou, *J. Electrochem. Soc.*, 2006, **153**, H15.
11 L. H. Chen, J. F. AuBuchon, A. Gapin, C. Daraio, P. Bandaru, S. Jin, D. W. Kim, I. K. Yoo and C. M. Wang, *Appl. Phys. Lett.*, 2004, **85**, 5373.
12 T. T. Tan, H. S. Sim, S. P. Lau, H. Y. Yang, M. Tanemura and J. Tanaka, *Appl. Phys. Lett.*, 2006, **88**, 103105.
13 W. Y. Sung, W. J. Kim, H. Y. Lee and Y. H. Kim, *Vacuum*, 2008, **82**, 551.
14 B. R. Huang, Y. K. Yang, T. C. Lin and W. L. Yang, *J. Nanomater.*, 2012, **2012**, DOI: 10.1155/2012/369763, article ID 369763, 6 pages.
15 M. Y. Chen, C. M. Yeh, J. S. Syu, J. Hwang and C. S. Kou, *Nanotechnology*, 2007, **18**, 185706.
16 C. K. Park, J. P. Kim, S. J. Yun, S. H. Lee and J. S. Park, *Thin Solid Films*, 2007, **516**, 304.
17 Y. Sakai, D. Tone, S. Nagatsu, T. Endo, S. Kita, F. Okuyama and N. Kobayashi, *Appl. Phys. Lett.*, 2009, **95**, 073104.
18 K. B. K. Teo, C. Singh, M. Chhowalla and W. I. Milne, *Encycl. Nanosci. Nanotechnol.*, 2003, **10**, 1.
19 L. Meng, J. Zhang and X. D. Zhu, *Thin Solid Films*, 2008, **516**, 2981.
20 W. H. Wang, Y. T. Lin and C. T. Kuo, *Diamond Relat. Mater.*, 2005, **14**, 907.
21 X. Fang, Y. Bando, U. K. Gautam, C. Ye and D. Golberg, *J. Mater. Chem.*, 2008, **18**, 509.
22 S. Zuo, X. Li, W. Liu, Y. He, Z. Xiao and C. Zhu, *J. Nanomater.*, 2011, **2011**, DOI: 10.1155/2011/382068, article ID 382068, 5 pages.
23 E. Stratakis, G. Eda, H. Yamaguchi, E. Kymakis, C. Fotakis and M. Chhowalla, *Nanoscale*, 2012, **4**, 3069.
24 Z. Ni, A. Ishaq, L. Yan, J. Gong and D. Zhu, *J. Phys. D: Appl. Phys.*, 2009, **42**, 075408.
25 H. Yamaguchi, K. Murakami, G. Eda, T. Fujita, P. Guan, W. Wang, C. Gong, J. Boisse, S. Miller, M. Acik, K. Cho, Y. J. Chabal, M. Chen, F. Wakaya, M. Takai and M. Chhowalla, *ACS Nano*, 2011, **5**, 4945.
26 K. Nose, R. Fujita, M. Kamiko and Y. Mitsuda, *Journal of Vacuum Science & Technology B: Microelectronics and Nanometer Structures*, 2012, **30**(1), 011204.
27 G. Shen, Y. Bando, C. Ye, B. Liu and D. Golberg, *Nanotechnology*, 2006, **17**, 3468.
28 H. Ago, T. Kugler, F. Cacialli, W. R. Salaneckm, M. S. P. Shaffer, A. H. Windle and R. H. Friend, *J. Phys. Chem. B*, 1999, **103**, 8116.
29 G. Y. Zhang, X. C. Ma, D. Y. Zhong and E. G. Wang, *J. Appl. Phys.*, 2002, **91**, 9324.
30 S. K. Srivastava, V. D. Vankar, D. V. S. Rao and V. Kumar, *Thin Solid Films*, 2006, **515**, 1851.
31 J. J. Li, Q. Wang and C. Z. Gu, *Ultramicroscopy*, 2007, **107**, 861.
32 P. J. Cao, Y. S. Gu, F. Liu, H. W. Liu, H. R. Zhang, F. Shen, Q. F. Zhang, D. Y. Zhong, J. Q. Li, S. Liu and H. J. Gao, *Appl. Phys. A: Mater. Sci. Process.*, 2005, **80**, 195.
33 S. K. Srivastava, V. D. Vankar and V. Kumar, *Nanoscale Res. Lett.*, 2008, **3**, 25.
34 N. G. Shang, C. P. Li, W. K. Wong, C. S. Lee, I. Bello and S. T. Lee, *Appl. Phys. Lett.*, 2002, **81**, 5024.
35 X. Ma, E. Wang, W. Zhou, D. A. Jefferson, J. Chen, S. Deng, N. Xu and J. Yuan, *Appl. Phys. Lett.*, 1999, **75**, 3105.
36 A. V. Melechko, K. L. Klein, J. D. Fowlkes, D. K. Hensley, I. A. Merkulov, T. E. McKnight, P. D. Rack, J. A. Horton and M. L. Simpson, *J. Appl. Phys.*, 2007, **102**, 074314.
37 C. E. Banks and R. G. Compton, *Analyst*, 2006, **131**, 15.
38 R. H. Fowler and L. Nordheim, *Proc. R. Soc. London, Ser. A*, 1928, **119**, 173.
39 J. Y. Huang, K. Kempa, S. H. Jo, S. Chen and Z. F. Ren, *Appl. Phys. Lett.*, 2005, **87**, 053110.
40 Q. Zhao, H. Z. Zhang, Y. W. Zhu, S. Q. Feng, X. C. Sun, J. Xu and D. P. Yu, *Appl. Phys. Lett.*, 2005, **86**, 203115.
41 R. Seelaboyina, J. Huang, J. Park, D. H. Kang and W. B. Choi, *Nanotechnology*, 2006, **17**, 4840.
42 U. N. Maiti, S. Maiti, T. P. Majumder and K. K. Chattopadhyay, *Nanotechnology*, 2011, **22**, 505703.
43 E. Stratakis, R. Giorgi, M. Barberoglou, Th. Dikonimos, E. Salernitano, N. Lisi and E. Kymakis, *Appl. Phys. Lett.*, 2010, **96**, 043110.
44 S. H. Lim, H. S. Kim, C. H. Lee, S. M. Pietruszko and J. Jang, *J. Non-Cryst. Solids*, 2002, **299**, 864.

